Mini-dystrophin Expression Down-regulates Overactivation of G Protein–mediated IP3 Signaling Pathway in Dystrophin-deficient Muscle Cells

Haouaria Balghi, Stéphane Sebille, Bruno Constantin, Sylvie Patri, Vincent Thoreau, Ludivine Mondin, Elise Mok, Alain Kitzis, Guy Raymond, and Christian Cognard

Institut de Physiologie et Biologie Cellulaires, CNRS UMR 6187, Université de Poitiers, 86022 Poitiers, France

We present here evidence for the enhancement of an inositol 1,4,5-trisphosphate (IP3) mediated calcium signaling pathway in myotubes from dystrophin-deficient cell lines (SolC1(−)) as compared to a cell line from the same origin but transfected with mini-dystrophin (SolD(+)). With confocal microscopy, we demonstrated that calcium rise, induced by the perifusion of a solution containing a high potassium concentration, was higher in SolC1(−) than in SolD(+) myotubes. The analysis of amplitude and kinetics of the calcium increase in SolC1(−) and in SolD(+) myotubes during the exposure with SR Ca^{2+} channel inhibitors (ryanodine and 2-APB) suggested the presence of two mechanisms of SR calcium release: (1) a fast SR calcium release that depended on ryanodine receptors and (2) a slow SR calcium release mediated by IP3 receptors. Detection analyses of mRNAs (reverse transcriptase [RT]-PCR) and proteins (Western blot and immunolocalization) demonstrated the presence of the three known isoforms of IP3 receptors in both SolC1(−) and SolD(+) myotubes. Furthermore, analysis of the kinetics of the rise in calcium revealed that the slow IP3-dependent release may be increased in the SolC1(−) as compared to the SolD(+), suggesting an inhibitory effect of mini-dystrophin in this signaling pathway. Upon incubation with pertussis toxin (PTX), an inhibitory effect similar to that of the IP3R inhibitor (2-APB) was observed on K^+-evoked calcium release. This result suggests the involvement of a Gi protein upstream of the IP3 pathway in these stimulation conditions. A hypothetical model is depicted in which both Gi protein and IP3 production could be involved in K^+-evoked calcium release as well as a possible interaction with mini-dystrophin. Our findings demonstrate the existence of a potential relationship between mini-dystrophin and SR calcium release as well as a regulatory role of mini-dystrophin on intracellular signaling.

The Journal of General Physiology

INTRODUCTION

Duchenne muscular dystrophy (DMD) is a progressive disease affecting 1/3,500 male births and characterized by the absence of dystrophin due to a defect in the p21 band of the X chromosome (Monaco et al., 1986). Dystrophin is a 427-kD cytoskeletal protein normally expressed at the inner surface of the sarcolemma of muscle fibers (Hoffman et al., 1987) and associated with a large complex of proteins known as the dystrophin-associated proteins (DAPs) (Ervasti and Campbell, 1991). In DMD patients, the lack of dystrophin leads to muscle degeneration and progressive weakness. Mutations of the dystrophin gene can also cause another pathology, the milder Becker muscular dystrophy (BMD) associated with the expression of a truncated 229-kD protein, namely mini-dystrophin, which lacks 17 units in the central rod domain. It has been shown that the small size of the gene encoding for this mini-dystrophin protein facilitated its expression via retroviral vector and allowed functional recovery in mdx mice (Deconinck et al., 1996).

Previous studies have shown association between increased cytosolic calcium and the extensive muscle degeneration at late stage DMD (Bodensteiner and Engel, 1978; Imbert et al., 1995). It has been proposed in dystrophic cells that the absence of dystrophin leads to an abnormal elevation of the cytosolic resting calcium level. However, the mechanism is poorly understood. Several authors suggested that dystrophin acts to favor the regulation or stabilization of calcium transport mechanisms in the sarcolemma (Imbert et al., 1996; Vandebrouck et al., 2001). Other studies reported some changes in the properties of membrane calcium currents in human DMD cells (Imbert et al., 2001). Presently, there is little data concerning a possible role of SR Ca^{2+} in the calcium mishandling observed in dystrophic cells (Liberona et al., 1998). Furthermore, modification of the regulation of calcium stores has been suggested to be involved in the general calcium disregulation in

Correspondence to Stéphane Sebille: stephane.sebille@univ-poitiers.fr

Abbreviations used in this paper: BMD, Becker muscular dystrophy; CICR, calcium-induced calcium release; DAP, dystrophin-associated protein; DHPR, dihydropyridine receptor; DMD, Duchenne muscular dystrophy; HD, half decay; HRP, horseradish peroxidase; IP3, inositol 1,4,5-trisphosphate; IP3R, IP3 receptor; IS, increase slope; PTX, pertussis toxin; ROI, region of interest; RT, reverse transcriptase; RYR, ryanodine receptor; TTP, time to peak.

mdx mice (Divet and Huchet-Cadiou, 2002; Vandebrouck et al., 2002).

In skeletal muscle, excitation–contraction coupling takes place by release of stored calcium from the SR via ryanodine receptors (RYRs). This release is triggered by an allosteric signal transmitted to the release channels from sarcolemmal voltage sensors, the dihydropyridine receptors (DHPRs) (Rios et al., 1991; Ursu et al., 2001; Lorenzon et al., 2004). Nevertheless, the inositol 1,4,5-trisphosphate receptor (IP3R) family of Ca^{2+} release channels, which play a key role in Ca^{2+} signaling in many other mammalian cells (Berridge, 1993; Blondel et al., 1994; Bootman et al., 1995; Furuichi and Mikoshiba, 1995), is thought to play a role in muscle cells. The process of IP3-induced Ca^{2+} release has been well documented in smooth muscle cells (Miyakawa et al., 1999; Patel et al., 1999; Dyer and Michelangeli, 2001). More controversial, however, is the idea that IP3 may modulate EC coupling in cardiac muscle (Lipp et al., 2000), which also remains poorly understood in skeletal muscle cells. Since the early works of Jaimovich and Hidalgo (Hidalgo et al., 1986), it is known that skeletal muscle fibers possess the basic molecular machinery for a functioning IP3 messenger system, including PLC, inositolphosphate phosphatases, IP3 kinase, and G-proteins (Carrasco and Figueroa, 1995).

In our previous work using a Sol cell line, intrinsically lacking dystrophin (Sol8 or SolC1(−)), we had selected stable Sol8 subclones, SolD(+), which constitutively express the BMD mini-dystrophin (Marchand et al., 2004). This study showed that myotubes from the SolC1(−) cell line exhibited morphological signs of cell death during myogenesis in culture, in parallel with an alteration of Ca^{2+} homeostasis. Furthermore, expression of BMD mini-dystrophin restored sarcolemmal expression and location of several members of the DAPs complex and allowed these cells to recover an intracellular Ca^{2+} concentration closer to myotubes from mouse primary cell culture.

We have observed that blockade of the IP3 pathway significantly reduced calcium release in SolC1(−). Hence, the aim of the present study was to examine calcium transients recorded on SolC1(−) and SolD(+) myotubes (Sol myotubes) during excitation by depolarization with a high potassium solution. RT-PCR, Western blot, and immunocytochemistry analyses have been performed to investigate the expression pattern of IP3R proteins in both myotubes, revealing the presence of a potential IP3-dependent calcium release system. Experiments conducted in this work demonstrate a modulator effect of mini-dystrophin (via a Gi protein) on IP3-dependent calcium release.

MATERIALS AND METHODS

Cell Lines

Sol8 myogenic cell line (a gift from I. Martelly, University of Paris XII, Creteil, France) was derived from the Sol8 cell line originally obtained from primary culture of normal C3H mouse soleus muscle (Mulle et al., 1988). The method for obtaining cell lines (SolC1(−) and SolD(+)) was described elsewhere (Marchand et al., 2004). In brief, after several steps of cloning, a dystrophin-deficient cell line was obtained, named SolC1(−). The SolD(+) cell line was obtained by transfection of the SolC1(−) cell line with a retrovirus encoding for mini-dystrophin (229 kD). SolC1(−) and SolD(+) cell lines ("Sol" cell lines in the following text) maintain a high ability to fuse and form myotubes. Cells were seeded on gelatin-coated glass coverslips in plastic dishes. Myoblasts were grown to ∼80% of confluence in HamF12/DMEM (1:1) medium supplemented with 10% FCS, 1% L-glutamine, and 1% antibiotics. To induce differentiation, the growth medium was changed to a fusion medium (DMEM supplemented with 2% heat-inactivated horse serum, insulin [10 μg/ml, Sigma-Aldrich]), 1% L-glutamine, and 1% antibiotics). Experiments were performed at the stage of F+4 for SolC1(−) and SolD(+) myotubes.

TABLE I

Description of Probes and Primers Used for RT-PCR

IP3R-1	
Forward primer	5′-TGG-CAG-AGA-TGA-TCA-GGG-AAA-3′
Reverse primer	5′-GCT-CGT-TCT-GTT-CCC-CTT-CAG-3′
Probe	5′-CCA-TGT-CCC-TGG-TCA-GCA-GCG-A-3′
IP3R-2	
Forward primer	5′-GCT-CAG-ATG-ATC-ACG-GAG-AAG-3′
Reverse primer	5′-ATC-TCA-TTT-TGC-TCA-CTG-TCA-CCT-3′
Probe	5′-CGA-GCC-ATG-TCA-CTT-GTC-AGC-AAC-G-3′
IP3R-3	
Forward primer	5′-TCA-TTG-TAC-TGG-TCC-GAG-TCA-AGA-3′
Reverse primer	5′-GCG-GGA-ACC-AGT-CCA-GGT-3′
Probe	5′-CCG-GCC-CCG-AGA-GCT-ATG-TGG-CT-3′

RT-PCR

Reverse Transcription. Total cellular RNA was extracted using RNABle kit (Eurobio). RNAs (10 μL) were reverse transcribed in a 25-μl reaction mixture consisting of first strand buffer (25 mM Tris, pH 8.3, 37.5 mM KCl, 1.5 mM $MgCl_2$), 10 mM DTT, 1 mM each dNTP, 2.4 mg of random hexamers, 40 U RNase inhibitor (RNA guard, Amersham Biosciences), and 400 U M-MLV reverse transcriptase (GIBCO-BRL). Reverse transcription was performed at 37°C for 60 min followed by 2 min at 100°C. The solution was then diluted twice in water.

Real-time PCR. The 15-μl reaction mixture contained 7.5μl 2× Taqman Universal Master Mix (Applied Biosystems), 5 μl of RT products, and appropriate primers and probes (900 nM and 200 nM, respectively). All probes contained a 3′ TAMRA (6-carboxy-tetramethylrhodamine) quencher dye and were labeled at the 5′ end with a FAM (6-carboxyfluorescein) reporter fluorescent dye. Probes and primers are described in Table I.

Amplification was performed at 50°C for 2 min, 95°C for 10 min, followed by 40 cycles at 95°C (15 s) and 60°C (1 min). Reactions were performed in MicroAmp optical 96-well reaction plates (Applied Biosystems) using an ABI PRISM 7700 sequence detection system (Applied Biosystems). All measurements were normalized to the mitochondrial ribosomal protein S6 (Mrps6, an endogenous control) to account for the variability in the initial concentration and quality of the total RNA.

SDS-PAGE and Immunoblot

Total cell lysates were obtained from SolC1(−) and SolD(+) myotubes. Cells were washed with PBS and solubilized at 4°C in lysis

buffer containing 50 mM Tris-HCl (pH 7.5), 1 mM EDTA, 100 mM NaCl, 1% Triton X-100 and protease inhibitors (20 μM leupeptin, 0.8 μM aprotinin, 10 μM pepstatin, and 2 mM 4-[2-aminoethyl]-benzenesulfonyl fluoride). Cells were scraped from the dishes and, after incubation on ice for 30 min, clarified by centrifugation at 15,000 *g* for 5 min at 4°C. Total proteins were quantified using the Bio-Rad Laboratories protein assay reagent and 30 μg of protein was loaded onto an SDS-PAGE apparatus. Proteins were separated in 5% polyacrylamide gels and electrophoretically transferred from gels to a 0.20-μm pore nitrocellulose membrane (Sartorius) using a Miniprotean III electroblotter (Bio-Rad Laboratories) for 2 h at 4°C. Immunoblots were washed in PBS containing 0.1% Tween-20 (PBS-Tween) and then probed overnight at 4°C with primary antibodies: a rabbit polyclonal antibody raised against IP3R-1 (Affinity Bioreagents), a goat polyclonal antibody raised against IP3R-2 (1:1,000; Santa Cruz Biotechnology), and a mouse monoclonal antibody against IP3R-3 (1:1,000; BD Transduction Laboratories) in PBS-Tween. Membranes were washed and incubated for 1 h at 4°C with the secondary antibodies: either horseradish peroxidase–conjugated (HRP) anti-mouse (1:3,000; Jackson ImmunoResearch Laboratories) or HRP-conjugated anti-goat (1:2,000; Santa Cruz Biotechnology), or HRP-conjugated anti-rabbit (1:3,000; Amersham Biosciences). Bound antibodies were detected using enhanced luminol and oxidizing reagents as specified by the manufacturer (ECL; Amersham Biosciences).

Immunological Staining

Cultured cells were stained by an indirect immunofluorescence method. Cells were rinsed in TBS (20 mM Tris base, 154 mM NaCl, 2 mM EGTA, 2 mM $MgCl_2$, pH 7.5) and fixed with either 4% paraformaldehyde (PFA) in TBS for 20 min or methanol (stored at −20°C) for 6 min, at room temperature. Only samples fixed with PFA were permeabilized with TBS/0.5% Triton X-100 for 10 min. Affinity Bioreagents supplied the anti–IP3R-1 (the same was used for Western blot) and the anti–IP3R-2 epitope-affinity purified polyclonal antibodies (1:250, PA1-901; and 1:100, PA1-904, respectively). No commercial anti–IP3R-3 antibody was available for us to perform immunolocalization of this isotype. Cells were incubated with primary antibodies in TBS/1% BSA (Sigma-Aldrich) for 1 h. After washing in TBS, cells were incubated for 30 min with the secondary antibody rhodamine red-X–conjugated goat anti-rabbit (1:200; Jackson ImmunoResearch Laboratories). Samples were mounted in Vectashield Medium (Vector Laboratories Inc.) for viewing with a confocal laser scanning microscope using a Bio-Rad Laboratories MRC 1024. Immunostaining images were processed (no gamma adjustment) and assembled in Powerpoint 2000.

Confocal Ca^{2+} Measurement

Ca^{2+} activity was recorded by confocal laser scanning microscopy using a Bio-Rad Laboratories MRC 1024 equipped with a 15 mW Ar/Kr gas laser. The confocal unit was attached to an inverted microscope (Olympus IX70). Fluorescence signal collection was performed through the control software Lasersharp 3.2 (Bio-Rad Laboratories). Myotubes were loaded with 3 μM fluo-4 acetoxymethyl (AM) ester (Molecular Probes) for 15 min at room temperature (20°C) in a resting solution (130 mM NaCl, 5.4 mM KCl, 2.5 mM $CaCl_2$, 0.8 mM $MgCl_2$, 10 mM HEPES, and 5.6 mM glucose, pH 7.4).

The fluorescent images were visualized through the X60 oil immersion objective and collected every 300 ms (256 × 256). Regions of interest (ROIs) have been selected in myotubes, and fluorescence transients from these ROIs were analyzed. Myotubes exposed to high K^+ solution (47 mM KCl) were depolarized by an immediate change of solution by perifusion inducing global Ca^{2+} variations. Ryanodine (Sigma-Aldrich) was incubated at 100 μM for 10 min to inhibit RYRs. For IP3 inhibition studies, myotubes were incubated for 30 min in 50 μM 2-APB (Calbiochem) or for 20 min in the presence of 10 μM U73122 (Sigma-Aldrich). PTX (Calbiochem) was incubated at 1 μg/ml for 1 h.

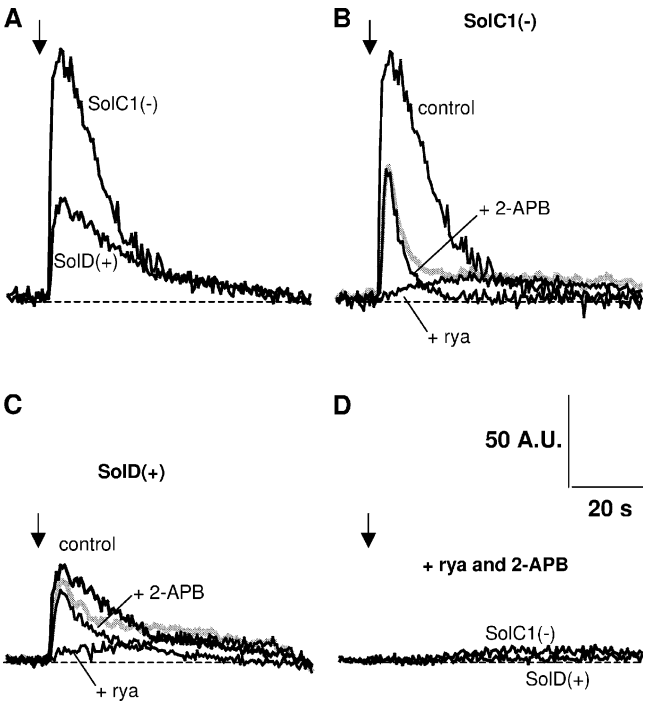

Figure 1. Examples of K^+-evoked calcium increase in SolC1(−) and SolD(+) myotubes: effects of ryanodine and 2-APB. Fluorescence rise from fluo-4–loaded myotubes was recorded as described in MATERIALS AND METHODS. During the recording, high K^+-containing solution (47 mM) was perifused near the analyzed myotubes (black arrows), and measurements were stopped after recovery to basal levels. (A) Representative examples of K^+-evoked calcium increase in a SolC1(−) and a SolD(+) myotube in control conditions. Examples of K^+-evoked calcium increase in the presence of ryanodine (+rya, 100 μM) or 2-APB (+2-APB, 50 μM) in SolC1(−) (B) and in SolD(+) (C). The gray curve represents the sum of the curve in the presence of ryanodine and the curve in the presence of 2-APB in SolC1(−) (B) and in SolD(+) (C). (D) Fluorescence signals obtained in SolC1(−) and SolD(+) myotubes with a combined incubation with ryanodine and 2-APB (+rya +2-APB).

Calcium Transient Processing

Fluorescence transients from ROIs in Fluo-4–loaded myotubes were analyzed with a computer program developed in our laboratory under IDL 5.3 structured language on a PC computer. Five parameters were extracted from analyzed curves for the characterization of calcium release amplitude and kinetics. These parameters were amplitude of the signal (normalized difference between the fluorescence of the peak and the background), area under the curve (area, in arbitrary units [A.U.s]) of the normalized curve, time to peak (TTP, in s), mean derivative at the beginning of the increase (increase slope, in A.U.s), and the half decay time (HD, in s). All these parameters were represented in histograms as relative values to control conditions in SolD(+) set at 1.0.

Statistical Analysis

All results are expressed as mean ± SEM of *n* observations. Sets of data were compared using Student's *t* test. All statistical tests

were performed using GraphPad Prism version 3.0 for Windows (GraphPad Software).

RESULTS

Calcium Increase Induced by Depolarizing Solution in SolC1(−) and SolD(+) Myotubes

Previous studies provided evidence for at least two phases in the calcium rise observed in cultured skeletal muscle cells exposed to a high potassium solution (Jaimovich et al., 2000; Powell et al., 2001). According to their kinetic properties, these two phases were identified as slow and fast calcium signals. In these works, the slow calcium signal was eliminated in the presence of IP3 inhibitors while the fast signal was abolished with ryanodine, showing also that the calcium increase observed in this stimulation condition was mainly originating from SR release.

We investigated here intracellular calcium increase during stimulation with a similar extracellular potassium solution (47 mM KCl) in fluo-4–loaded SolC1(−) (without dystrophin) and SolD(+) myotubes (expressing mini-dystrophin). Fig. 1 displays examples of fluorescence recordings in both cell types and in the presence of SR Ca^{2+} channels inhibitors. Upon superfusion with high potassium solution, in control conditions, all myotubes exhibited an intracellular calcium increase (K^+-evoked calcium increase) followed by a slow recovery but rarely showed a biphasic pattern (Fig. 1 A). Furthermore, the amount of released calcium was higher in SolC1(−) myotubes than in SolD(+) myotubes.

To understand the pathways of K^+-evoked calcium release in the Sol myotubes, we tested the effect of ryanodine and 2-APB separately in SolC1(−) (Fig. 1 B) and in SolD(+) (Fig. 1 C) as well as together in both myotube types (Fig. 1 D). Ryanodine, known to inhibit RYRs at high concentrations (preincubation: 100 μM for 15 min), induced a weak and slow K^+-evoked calcium increase in both SolC1(−) and SolD(+) myotubes (Fig. 1, B and C). Furthermore, the remaining transients in the presence of ryanodine as illustrated here were seen in >80% of the cells in SolC1(−) and in 50% of SolD(+). No signal was seen in all other tested cells. This difference between cells suggests a stronger sensitivity to ryanodine in SolD(+) for the K^+-evoked calcium release. Interestingly, the slow phase observed here closely resembled that initially presented in the study from Powell et al. (2001). To investigate the involvement of IP3Rs in K^+-evoked calcium release, the direct inhibitor of IP3 receptors, 2-APB, was also tested (preincubation: 50 μM for 30 min) on K^+-evoked calcium release in SolC1(−) (Fig. 1 B) and in SolD(+) (Fig. 1 C). In both cell types, the amplitude and amount of calcium release were notably reduced. Moreover, in both myotubes, calcium increase kinetics were not modified by 2-APB while the recovery of fluorescence

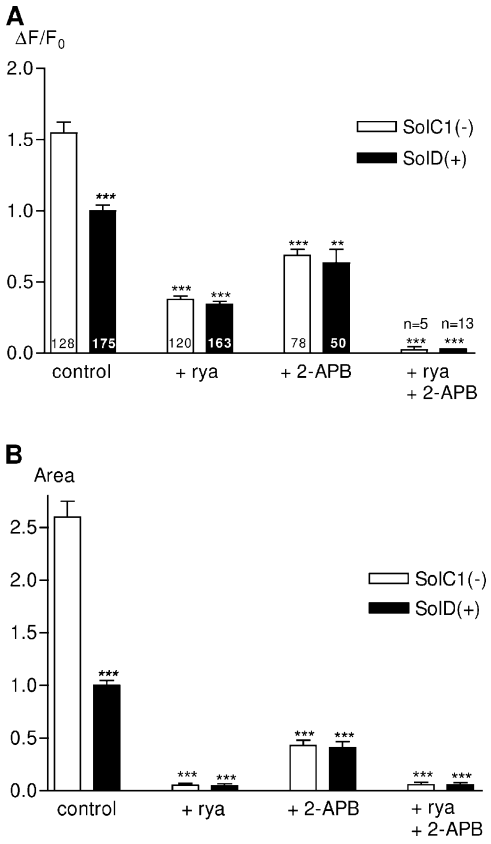

Figure 2. Amplitude and "area under the curve" parameters from K^+-evoked calcium increases in Sol cell lines: effects of ryanodine and 2-APB. Large-scale analysis of K^+-evoked fluorescence rises has been realized to compare them in the two myotube types and in the presence of SR Ca^{2+} channel inhibitors. All these parameters were represented in histograms as relative values to control conditions in SolD(+) set at 1.0. Parameters have been automatically measured with a computer program developed under IDL 5.3 (Fig. 3, inset). (A) Histogram representing the rise amplitude (ΔF/F0) in SolC1(−) (white bars) and SolD(+) (black bars) in controls and with inhibitors (same incubation conditions as in Fig. 1). The number of analyzed myotubes is given in histogram bars. (B) Histogram representing the "area under the curve" parameter measured on curves obtained in SolC1(−) (white bars) and SolD(+) (black bars). Each bar graph corresponds to the mean value ± SEM obtained for each type of myotube. ns, not significantly different. ***, $P < 0.001$; **, $0.001 \leq P < 0.01$; *, $0.01 \leq P < 0.05$ (Student's unpaired *t* test).

was faster than in control conditions. Finally, preincubation with both inhibitors together nearly abolished calcium release in Sol myotubes (Fig. 1 D).

Thus, although SolC1(−) and SolD(+) myotubes did not show a biphasic K^+-evoked calcium release, the inhibition of RYRs revealed a slow phase of calcium release while the blockade of IP3Rs, showed a fast phase. Both inhibitions together led to a nonsignificant calcium increase, suggesting that this response mainly depends on the SR release in SolC1(−) and SolD(+) myotubes.

A reconstructed release curve obtained by adding together the curve in the presence of ryanodine and the

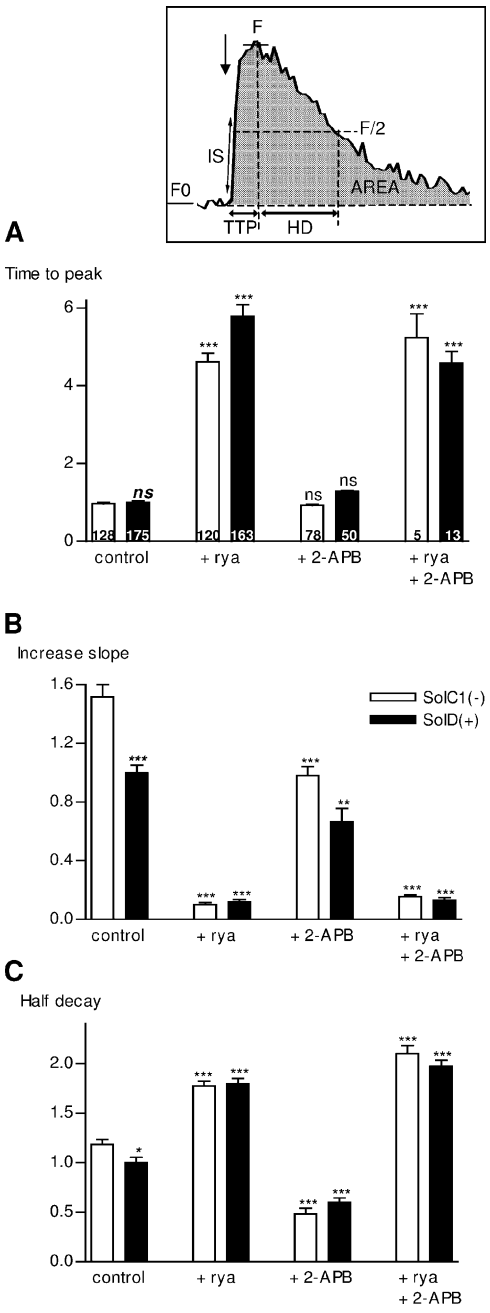

Figure 3. Kinetics parameters from K^+-evoked calcium increases in Sol cell lines: effects of ryanodine and 2-APB. Inset, measurement of amplitude and kinetic parameters. All these parameters were automatically measured with a computer program developed in our laboratory under IDL 5.3 structured language. F0, basal fluorescence obtained from averaged fluorescence before high K^+ stimulation. After stimulation, a maximum value is detected in the curve and fluorescence around this value was averaged, giving the F value. Amplitude was determined as F−F0/F0 (ΔF/F0). Area under the curve (area, A.U.s.) was calculated in integrating the curve. Time to peak (TTP, in seconds) was determined as the time between 5% of F and F during the increase. Half decay time (HD, in seconds) was determined as the time between F and F/2 during the decay. Increase slope (in A.U/s) was determined in averaging the derivative of the curve where it was the maximum during the increase, corresponding to the beginning of the increase. All these parameters were represented in histograms as relative values to control conditions in SolD(+) set at 1.0. (A) Histogram representing the "time to peak" parameter in SolC1(−) (white bars) and SolD(+) (black bars) in controls and with inhibitors. The number of analyzed myotubes is given on histogram bars. Histograms representing the "increase slope" (B) and the "half decay" (C) parameters. Each bar graph corresponds to the mean value ± SEM obtained for each type of myotubes. ns, not significantly different. ***, $P < 0{,}001$; **, $0.001 \leq P < 0.01$; *, $0.01 \leq P < 0.05$ (Student's unpaired *t* test).

curve in the presence of 2-APB is presented in Fig. 1 B for SolC1(−) and in Fig. 1 C for SolD(+) myotubes (in gray). This reconstructed curve corresponds to the sum of both the ryanodine-insensitive and the 2-APB–insensitive SR release components. In SolC1(−), the sum of the two release components was clearly weaker than the control (Fig. 1 B), suggesting a positive interaction between the two SR release mechanisms. In SolD(+), the difference between the sum of the two release components and the control was less obvious (Fig. 1 C).

K^+-evoked Calcium Increase Depends on Two Release Components

To explore the two release phases in both cell lines, large-scale analysis has been performed on K^+-evoked calcium recordings. Two parameters have been measured to investigate calcium releases: amplitude (normalized difference between the fluorescence of the peak and the background, $\Delta F/F_0$) and area under the curve (A.U.s) (Fig. 2). To simplify comparisons between myotube types and inhibitor exposure, the following results will be given relative to control conditions with SolD(+) set at 1.0. As compared with SolD(+) (black bars), SolC1(−) myotubes (white bars) displayed increased calcium with respect to amplitude (Fig. 2 A) and area under the curve (Fig. 2 B).

In the presence of ryanodine, calcium rise was reduced in SolC1(−) and SolD(+) as shown by a reduction in amplitude (76% and 66% reduction, respectively; Fig. 2 A) and area under the curve (97% and 95% of reduction, respectively; Fig. 2 B). Nevertheless, no significant difference in calcium release was found in the two cell types incubated with ryanodine (with respect to ΔF/F0 and area under the curve). These results suggest the presence of a calcium release mechanism insensitive to ryanodine, which is more apparent in SolC1(−), during the excitation–calcium release coupling.

Large-scale analysis of calcium rise in SolC1(−) and SolD(+) myotubes also demonstrated that 2-APB exposure significantly reduced calcium increase amplitude (61% and 37% of reduction, respectively; Fig. 2 A) and area under the curve (75% and 59% reduction, respectively; Fig. 2 B). This result suggests that calcium release in SolC1(−) myotubes was more affected by the IP3R inhibitor versus SolD(+) myotubes. It is also worth noting that in control conditions, there was a significant

difference in calcium release between SolC1(−) and SolD(+), whereas with 2-APB application, calcium release was similar between the two myotube types. Furthermore, combination of ryanodine and 2-APB further reduced calcium release in both myotubes (>95% reduction; Fig. 2, A and B).

Identification of Both Fast and Slow Components in K^+-evoked Calcium Increase

Kinetic parameters, derived from the fluorescence signals, were examined to further compare the calcium release pattern in responding SolC1(−) and SolD(+) myotubes (Fig. 3). The parameters defined here were the time to peak (TTP, in seconds) (Fig. 3 A), the mean derivative during the increase (increase slope [IS], $A.U.s^{-1}$) (Fig. 3 B), and the half decay (HD, in seconds) of fluorescence (Fig. 3 C).

In our experiments, the TTP and IS parameters provided information mainly on mechanisms that initiate calcium release. Fig. 3 A shows that in control conditions, TTP values were not significantly different between SolC1(−) and SolD(+) myotubes. This suggests that the mechanism involved in the triggering of SR calcium release, during depolarization, might not be different between SolC1(−) and SolD(+) myotubes. TTP measured in the presence of ryanodine was dramatically increased in both myotubes (375% and 489% increase, respectively; Fig. 3 A). These quantitative results raise the assumption that a slow rise in calcium increase, independent of RYR activation, could occur as a secondary calcium release. As compared with the controls, exposure with 2-APB did not significantly change the TTP parameter, suggesting that the first steps of this K^+-evoked calcium release may not be dependent on IP3 receptors. Kinetic parameters from incubation of ryanodine and 2-APB together are presented in Fig. 3 for a complete analysis. However, because of the weak calcium release revealed in these conditions, we did not further study the effect of incubation with ryanodine and 2-APB together. Because TTP depends on amplitude and because other mechanisms of Ca^{2+} buffering and SR uptake are activated when the intracellular calcium concentration is increased, we measured the slope of calcium rise (IS) at the beginning of the increase, when the opening of SR Ca^{2+} channels is the main process that leads to increased calcium concentrations. This parameter is increased in control SolC1(−) as compared with control SolD(+) myotubes (Fig. 3 B) and is significantly reduced in the presence of ryanodine in both cells (92% and 88% reduction, respectively, in SolC1(−) and SolD(+)). The inhibitory effect during IP3R blockade (2-APB) was weaker than with ryanodine exposure and leads to a similar decrease (versus control) in the IS parameter in both SolC1(−) and SolD(+) (35% and 33% decrease, respectively).

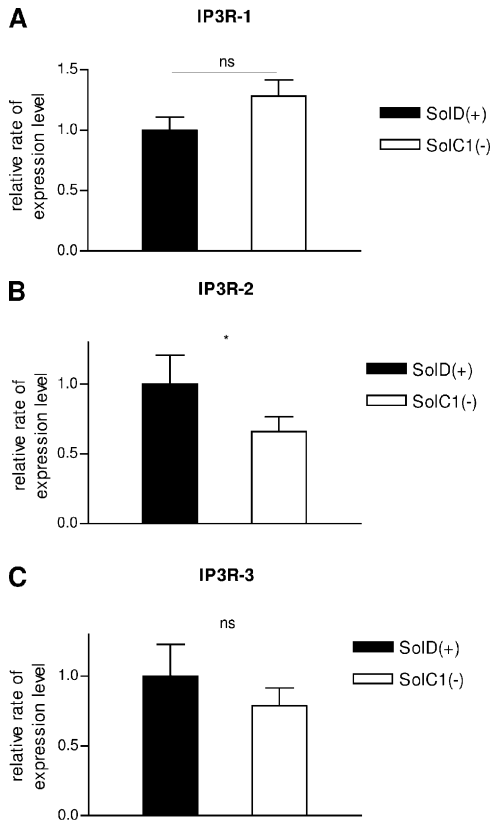

Figure 4. Expression of IP3Rs in SolC1(−) and SolD(+) myotubes. RT-PCR–based analysis of IP3R-1 (A), IP3R-2 (B), and IP3R-3 (C) mRNA for 40 cycles. S6 ribosomal mRNA was used as an internal standard. Relative mRNA expression levels of IP3R-1, IP3R-2, and IP3R-3 was compared with S6 ribosomal mRNA expression. Expression of IP3R isoforms in SolC1(−) myotubes were compared with normalized SolD(+) one. Each bar graph corresponds to the mean value ± SEM obtained for $n = 4$ (n number of experiments). ns, not significantly different. ***, $P < 0{,}001$; **, $0.001 \leq P < 0.01$; *, $0.01 \leq P < 0.05$ (Student's unpaired t test).

Fig. 3 C presents the half decay (HD) parameter, which represents the recovery of fluorescence to the basal level in treated and untreated Sol myotubes. In control conditions, the time to recover the basal level of fluorescence was longer in SolC1(−) than in SolD(+) myotubes, showing that the calcium rise in SolC1(−) myotubes lasted longer than in SolD(+) myotubes. When RYRs were inhibited with ryanodine, the HD was longer in both myotubes (78% and 80% increase in SolC1(−) and SolD(+), respectively; Fig. 3 C). Moreover, when calcium release from IP3Rs was blocked with 2-APB, the HD in SolC1(−) and SolD(+) myotubes was decreased (59% and 40% of reduction in SolC1(−) and SolD(+), respectively), leading to a faster recovery of fluorescence, particularly in SolC1(−).

Taken together, these results suggest that IP3Rs are involved in K^+-evoked calcium release in both SolC1(−) and SolD(+) myotubes. The analysis of kinetic parameters

permitted us to identify a fast (with 2-APB exposure) and a slow (with ryanodine exposure) component in K+-evoked calcium increase—the fast component being mediated by RYRs and the slow component being mediated by IP3Rs. Interestingly, both kinetic and amplitude parameters suggest that the slow component is enhanced in SolC1(−) myotubes where dystrophin is absent. To determine whether differences in calcium signaling could be attributed to the IP3 signaling pathway, we then examined the presence of IP3 receptors in Sol myotubes.

Expression and Localization of IP3Rs

Three different isoforms of IP3Rs are known to be present in skeletal muscle cells (De Smedt et al., 1997). IP3R-1 was demonstrated to be the minor form in skeletal muscle and in the Sol8 cell line; IP3R-2 is highly present in skeletal muscle, and IP3R-3 is the major isoform in the Sol8 cell line. mRNA expression of IP3R isoforms was examined in SolC1(−) and SolD(+) myotubes with quantitative RT-PCR. Fig. 4 shows that mRNA from IP3R-1 (Fig. 4 A), IP3R-2 (Fig. 4 B), and IP3R-3 (Fig. 4 C) was detected in both SolC1(−) and SolD(+) myotubes with no highly significant differences between SolC1(−) and SolD(+) for the three isotypes.

Expression of the IP3R proteins has also been investigated in SolC1(−) and SolD(+) myotubes with Western blot (Fig. 5 A). These qualitative experiments clearly demonstrated the presence of IP3R-1, IP3R-2, and IP3R-3 proteins in both SolC1(−) and SolD(+) myotubes.

Previous studies (Salanova et al., 2002) have shown that IP3Rs are localized in the longitudinal SR, which is the main site of localization of the SERCA pumps, ensuring the Ca^{2+} uptake mechanism. In cardiac muscle, the immunolocalization of RYRs and IP3Rs indicated that the IP3R-2 colocalized with part of the junctional RYR-2 (Lipp et al., 2000; Mackenzie et al., 2002). In our work, immunostaining experiments have been conducted in order to localize IP3R-1 and IP3R-2 in Sol myotubes (Fig. 5 B). Similar to what was observed in primary mouse cultures (Powell et al., 2001), a clear staining of IP3R-1 was found in SolC1(−) myotubes in the nuclear envelope region, as well as in the myoplasm (Fig. 5 B, a). In SolD(+) myotubes (Fig. 5 B, c), IP3R-1 was also localized in the nuclear envelope region but the staining was fainter than in SolC1(−) and a peripheral staining was also observed. For both SolC1(−) and SolD(+) myotubes, IP3R-2 was never found in the nuclear envelope region. In SolC1(−) (Fig. 5 B, b) and SolD(+) (Fig. 5 B, d), IP3R-2 showed a peripheral and fully cytoplasmic localization, and, as indicated with white arrows, striated staining pattern appeared at this differentiation stage (4 d in differentiation medium). These qualitative data demonstrate that IP3 receptors are expressed in SolC1(−) and SolD(+) myotubes. They also indicate localization of IP3R-1 near the nuclear envelope in both cells and a myoplasmic localization of IP3R2. Furthermore, because of the striated staining pattern observed in both myotube types, one can postulate that IP3R-2 is localized near the structures organized in striations (contractile proteins or SR) that take place at this differentiation stage in a skeletal muscle cell. Unfortunately, we were not able to localize the third isoform with the available IP3R-3 antibodies.

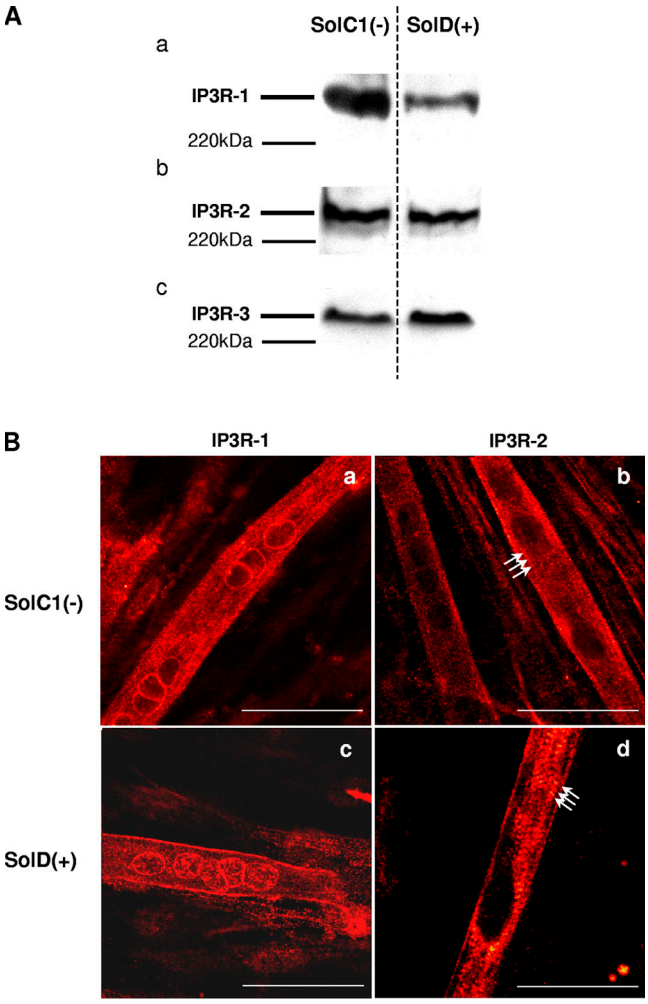

Figure 5. Determination and immunolocalization of the expression pattern of IP3R proteins. (A) Western blot analysis of IP3R-1 (a), IP3R-2 (b), and IP3R-3 (c), respectively, in SolC1(−) and SolD(+) myotubes. 30 μg protein from each type of myotube was separated on 5% SDS-PAGE, transferred onto a pore nitrocellulose membrane, and processed for Western blot analysis with specific antibodies. The 220-kD band corresponded to the molecular weight of the myosin protein. (B) IP3R isoform immunolabeling in SolC1(−) and SolD(+) myotubes was observed with laser scanning confocal microscopy. IP3R-1 and IP3R-2 localizations were detected using polyclonal antibodies, PA1-901 and PA1-904, respectively. IP3R-1 staining is localized in the nuclear envelope region and in the cytoplasm in SolC1(−) (a) and in SolD(+) (c) myotubes. IP3R-2 showed a peripheral and fully cytoplasmic localization and, as indicated with white arrows, striated staining pattern appeared at this differentiation stage in SolC1(−) (b) and SolD(+) (d) myotubes. Bars, 25 μm.

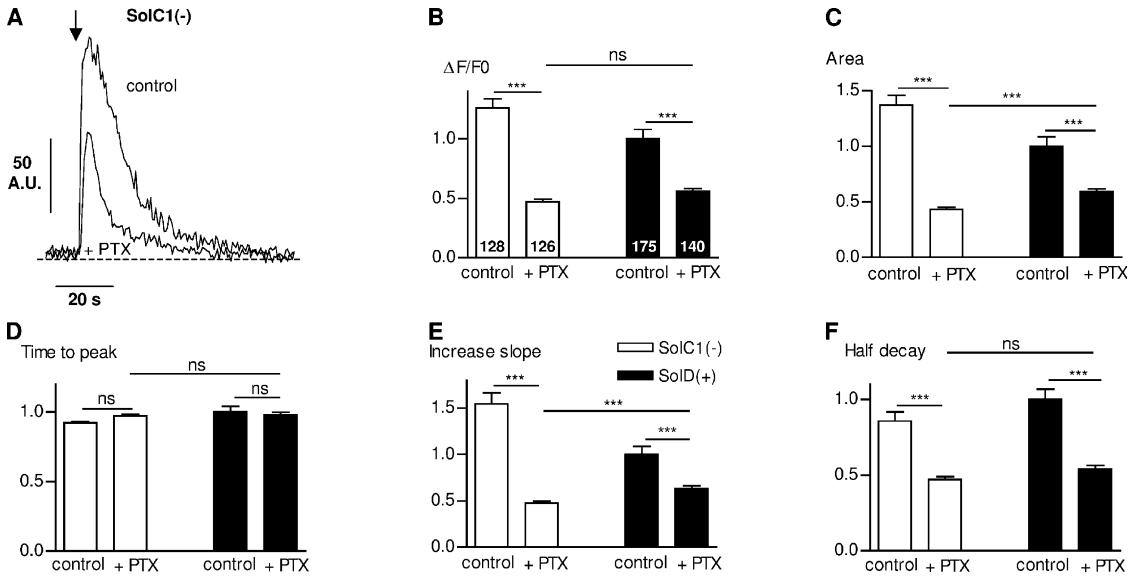

Figure 6. Effect of PTX on K+-evoked calcium increases in Sol cell lines. (A) Representative examples of K^+-evoked calcium increase in a SolC1(−) in control conditions and in the presence of PTX (+PTX, 1 μg/ml). Histograms representing the amplitude (ΔF/F0) (B) in SolC1(−) (white bars) and SolD(+) (black bars), the "area under the curve" parameter (C), time to peak (s) (D), increase slope (E), and half decay (F) in controls and with PTX exposure. The number of analyzed myotubes is given on histogram bars in B. ns, not significantly different. ***, $P < 0{,}001$; **, $0.001 \leq P < 0.01$; *, $0.01 \leq P < 0.05$ (Student's unpaired *t* test).

These above data are in agreement with the inhibitory effects of 2-APB during K^+-evoked calcium release in Sol myotubes, indicating the presence of an IP3-mediated system of calcium release in both SolC1(−) (lacking dystrophin) and SolD(+) (expressing mini-dystrophin) myotubes.

Effects of PTX

The skeletal muscle fiber possesses the basic molecular machinery for a functioning IP3 messenger system, including PLC, inositolphosphate phosphatases, IP3 kinase, and G proteins (Carrasco and Figueroa, 1995). The IP3 pathway involves PLC activation that catalyzes the hydrolysis of phosphoinositol 4,5 bisphosphate (PIP2), producing diacylglycerol and IP3. Recent investigations have shown that a Gi protein could be involved in Ca^{2+} release induced by depolarization via the activation of PLC (Araya et al., 2003). We observed with the use of a PLC inhibitor (U73122) a significant decrease of K^+-evoked calcium release in Sol myotubes (unpublished data). To test the involvement of a G protein in K^+-evoked calcium release, we tested the effect of PTX, known to inactivate several G proteins via ADP-ribosylation of their α subunits (Lampe et al., 2001), on depolarization-induced Ca^{2+} transients (Fig. 6). Fig. 6 A shows an example of K^+-evoked calcium increase obtained in SolC1(−) myotubes in the presence of 1 μg/ml PTX. PTX decreased Ca^{2+} release amplitude and modified Ca^{2+} release kinetics in SolC1(−) myotubes. Amplitude and kinetic parameters have been measured in a large-scale analysis to examine the inhibitory effect of PTX (Fig. 6, B–F). PTX significantly reduced the amplitude (Fig. 6 B) and the area under the curve (Fig. 6 C) of K^+-evoked calcium release (63% and 69% decrease, respectively) in SolC1(−) (white bars) and to a lesser extent (44% and 41% decrease, respectively) in SolD(+) myotubes (black bars). Moreover, as with 2-APB, PTX did not modify time to peak in both myotubes (Fig. 6 D). Also, PTX showed a similar decrease in the increase slope (Fig. 6 E) as shown with 2-APB. PTX also decreased the half decay in SolC1(−) (45%) and in SolD(+) (46%) myotubes (Fig. 6 F). Thus, exposure with either 2-APB or PTX led to the same pattern of calcium release kinetics. These results favor the involvement of a Gi protein acting upstream of an IP3-mediated K^+-evoked calcium release. Furthermore, despite the differences between SolC1(−) and SolD(+) in K^+-evoked calcium rise, application of both 2-APB and PTX led to similar patterns of release in both myotube types.

Taken together, these data demonstrate an involvement of the IP3 pathway in Sol myotubes after membrane depolarization as well as an overactivation of the Gi protein–dependent pathway in myotubes lacking dystrophin as compared with cells in which mini-dystrophin has been introduced.

DISCUSSION

In this work, we performed experiments on two types of myotubes originating from the same Sol8 cell line: (1) dystrophin-deficient myotubes, SolC1(−), and

(2) myotubes transfected to express the BMD mini-dystrophin, SolD(+). This mini-dystrophin restoration allows the readdressing of members of the DAP complex and the recovery of intracellular Ca^{2+} levels similar to those observed in myotubes from mouse primary cell culture (Marchand et al., 2004). Furthermore this model allows the physiological exploration of two cellular systems with the only difference being the presence (or not) of mini-dystrophin.

We provided here evidence that K^+-evoked calcium rise was very different between these two cell types and these differences were almost abolished with addition of IP3 pathway inhibitors. RT-PCR, Western blot, and immunocytochemistry analyses demonstrated the presence of the three IP3R isoforms in both myotubes and subsequently the presence of IP3-dependent release machinery. Furthermore, experiments with the aim to "dissect" K^+-evoked calcium rise by means of SR calcium release channel inhibitors revealed two types of release: (1) a fast release that depended on RYRs and (2) a slow release that was mediated by IP3Rs. The main difference between SolC1(−) and SolD(+) was a higher IP3R-dependent component in SolC1(−). In these stimulation conditions, the presence of mini-dystrophin seemed to have an inhibitory effect on IP3-dependent pathway probably through modulation of a Gi protein.

Involvement of Two Excitation–Calcium Release Processes

The excitation–contraction coupling system in skeletal muscle involving DHPRs/RYRs has been largely investigated (Cognard et al., 1990, Franzini-Armstrong and Kish, 1995; Protasi et al., 2002). In our experiments, the use of high concentration ryanodine did not completely abolish Ca^{2+} release in SolC1(−) and SolD(+) myotubes, suggesting a component of release independent of RYRs. A previous study performed on dyspedic muscle myotubes, which do not express RYR isoforms and lack excitation–contraction coupling, demonstrated the absence of a fast component of calcium release but the presence of a slow IP3-dependent calcium release component, particularly in the nucleus (Estrada et al., 2001). This study along with others from Jaimovich's group (Jaimovich et al., 2000; Powell et al., 2001), using primary cultures from rat and mouse muscle, suggest that skeletal muscle cells in development display a significant calcium release mechanism from IP3Rs after membrane depolarization. In our work, although we did not observe a biphasic K^+-evoked calcium rise, considerable differences in kinetics, with inhibitor exposure, strongly support the presence of two processes of excitation–calcium release coupling in Sol cells. Experiments with a K^+ perfusion system at a lower rate frequently displayed two more phases in the K^+-evoked calcium rise (unpublished data), suggesting that the rate of membrane depolarization plays a role in the separation of these two phases.

IP3 Inhibitors Reduced Differences in K^+-evoked Calcium Rise between SolC1(−) and SolD(+) Cells

Our first observation was that depolarization of dystrophin-deficient myotubes (SolC1(−)) induced a larger intracellular calcium increase as compared with the SolD(+) (expressing mini-dystrophin). This suggests that mini-dystrophin expression could play a regulatory role in calcium release during cell excitation. Moreover, exposure to IP3 inhibitors led to a higher decrease of K^+-evoked calcium release in SolC1(−) as compared with SolD(+), and the pattern of release obtained in these conditions was similar between the two cells. This suggests that the presence of mini-dystrophin could be related to the specific reduction of IP3R-dependent K^+-evoked calcium release. One can then hypothesize that the enhanced calcium release in dystrophin-deficient myotubes could be due for the most part to the activation of the IP3-dependent release process that is missing or depressed in mini-dystrophin–expressing myotubes.

Interaction between RYR-dependent and IP3R-dependent Releases?

Given that the exposure to a mixture of 2-APB and ryanodine almost abolished the K^+-evoked calcium increase, it was surprising to observe that the sum of releases, induced by separate applications of the two compounds, did not result in the release observed in the controls (Fig. 1, B and C, and Fig. 2), particularly in SolC1(−). Furthermore, increase kinetics (with respect to TTP and IS) were similar in controls and in cells exposed to 2-APB, suggesting that the fast release from RYRs was unchanged in both conditions. It is well known that release from IP3Rs strongly depends on intracellular calcium concentrations, leading to a calcium-induced calcium release (CICR) with high levels of Ca^{2+} (Berridge, 1993). It is possible that in control conditions, calcium ions initially released from RYRs may activate IP3Rs and then amplify the slow release mediated by the IP3 pathway. The IP3-dependent release observed in the presence of ryanodine is thus reduced as compared with control conditions, particularly in SolC1(−) in which the IP3-dependent release is pronounced.

Inhibitory Effect of Mini-dystrophin in the IP3 Production Pathway

Liberona et al. (1998) previously observed that in dystrophic cells, basal levels of IP3 mass were three to six-fold higher than in their normal counterparts. Moreover, other studies demonstrated increased IP3 mass with depolarization, showing that the level of IP3 mass in cultured muscle cells could be regulated by membrane potential, through the α-1 subunit of the DHPR (Araya et al., 2003) and by muscarinic acetylcholine receptors (Reyes and Jaimovich, 1996). Our experiments, combined with this data, lead us to think that IP3 production

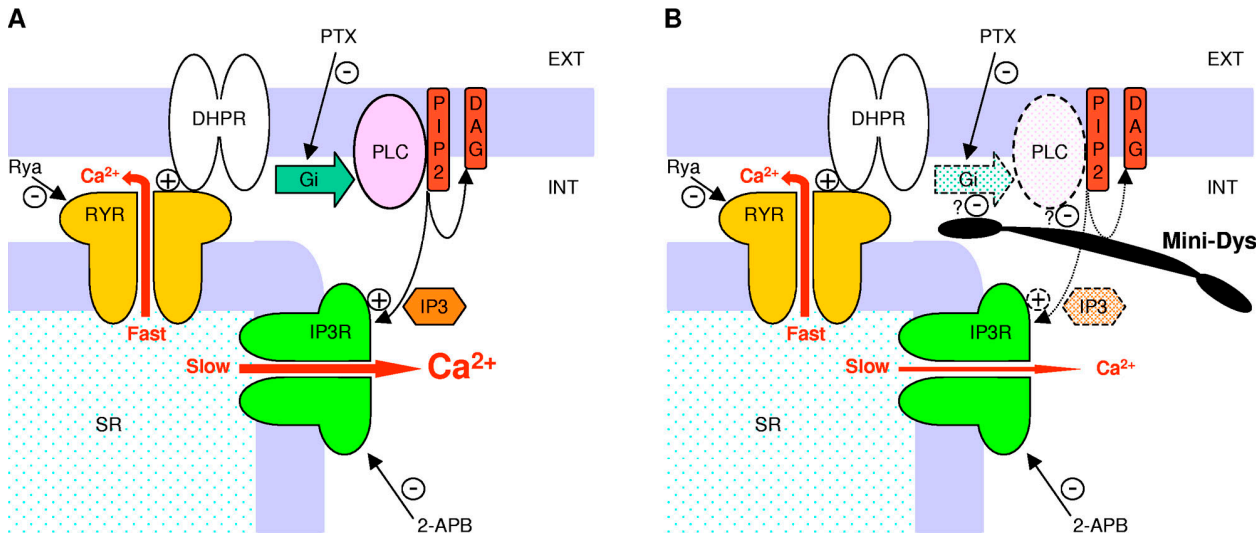

Figure 7. A proposed hypothetical model of the mini-dystrophin reduction effect on PLC activity. (A) During depolarization, the activation of DHPRs, followed by calcium release from RYRs (described as fast) would also stimulate PLC through Gi protein (Araya et al., 2003). The IP3, produced from the PLC activity, reaches IP3Rs from the SR and leads to calcium release (slow). (B) The presence of the mini-dystrophin protein would repress the activity of PLC via the Gi protein and consequently reduce the slow release from IP3 receptors.

after membrane depolarization is significantly elevated in dystrophin-deficient myotubes and that the presence of mini-dystrophin under the membrane leads to reduced IP3 production.

The mechanism by which membrane depolarization induces the activation of PLC to produce IP3 has not been established. Specific G protein βγ dimers are thought to mediate the regulation of PLC activity in some cases (Kanthou et al., 1996) and it was proposed that in skeletal muscle, the voltage sensor DHPR could directly or indirectly be linked to a protein of the Gi type, which in turn activates a PLC (Araya et al., 2003). The results obtained here with PTX on depolarization-evoked calcium release demonstrate a strong reduction in calcium release that was more pronounced in SolC1(−) than in SolD(+). We then suggest an inhibitory effect of mini-dystrophin at that level and propose a hypothetical model of the effect of mini-dystrophin on IP3 production (Fig. 7). During membrane depolarization, DHPRs could both activate the release from RYRs (fast release) and enhance the activity of PLC through a Gi protein. This enhanced activity leads to an increase in IP3 concentration in the cytoplasm and induces calcium release from IP3Rs (slow release) (Fig. 7 A). The presence of mini-dystrophin under the membrane could result in a reduction of PLC activity at the level of PLC, or upstream of the Gi protein (Fig. 7 B). Concerning the possible link between mini-dystrophin and these proteins, the binding between heterotrimeric G proteins and syntrophin (a cytoskeletal protein known to interact with dystrophin) has been demonstrated in skeletal muscle cells (Zhou et al., 2005). These scaffolding proteins involved in the protein network under the membrane could have modulatory effects on signaling activities. One can postulate that a negative protein–protein interaction involving these scaffolding proteins could be restricted to the submembrane area where this complex is located. Nevertheless, if IP3 production is reduced, a reduced Ca^{2+} release will follow, and the consequences of the negative interaction could be propagated inwards through the reduction of the diffusible CICR mechanism. Conversely, the absence of dystrophin may have the opposite effect in enhancing the CICR mechanism, even in thicker structures, such as adult muscle fibers.

Three main findings are of particular interest in this work: first, this study indicates a possible role of Ca^{2+} release from the SR in Ca^{2+} mishandling in dystrophin-deficient cells. Specifically, our results strongly support the hypothesis of increased Ca^{2+} release in dystrophin-deficient myotubes, leading to calcium deregulation. Second, this deregulation can be attenuated with mini-dystrophin expression (a candidate for gene therapy). Finally, this work shows evidence for a major role of the IP3 pathway in Ca^{2+} release during stimulation in dystrophin-deficient myotubes.

The authors thank Prof. Isabelle Martelly (University of Paris XII, Créteil, France) for providing the original Sol8 cell line. We thank Françoise Mazin for her expert technical assistance in cell culture and Anne Cantereau for her expert technical assistance in confocal microscopy.

This work was financially supported by grants from Centre National de la Recherche Scientifique (CNRS UMR 6187), University of Poitiers, and the Association Française contre les Myopathies. This work is part of the thesis project of Haouaria Balghi

supported by a fellowship from the Association Française contre les Myopathies.

Angus C. Nairn served as editor.

Submitted: 8 November 2005
Accepted: 27 December 2005

REFERENCES

Araya, R., J.L. Liberona, J.C. Cardenas, N. Riveros, M. Estrada, J.A. Powell, M.A. Carrasco, and E. Jaimovich. 2003. Dihydropyridine receptors as voltage sensors for a depolarization-evoked, IP3R-mediated, slow calcium signal in skeletal muscle cells. *J. Gen. Physiol.* 121:3–16.

Berridge, M.J. 1993. Inositol trisphosphate and calcium signalling. *Nature.* 361:315–325.

Blondel, O., G.I. Bell, M. Moody, R.J. Miller, and S.J. Gibbons. 1994. Creation of an inositol 1,4,5-trisphosphate-sensitive Ca^{2+} store in secretory granules of insulin-producing cells. *J. Biol. Chem.* 269:27167–27170.

Bodensteiner, J.B., and A.G. Engel. 1978. Intracellular calcium accumulation in Duchenne dystrophy and other myopathies: a study of 567,000 muscle fibers in 114 biopsies. *Neurology.* 28:439–446.

Bootman, M.D., L. Missiaen, J.B. Parys, H. De Smedt, and R. Casteels. 1995. Control of inositol 1,4,5-trisphosphate-induced Ca^{2+} release by cytosolic Ca^{2+}. *Biochem. J.* 306(Pt 2):445–451.

Carrasco, M.A., and S. Figueroa. 1995. Inositol 1,4,5-trisphosphate 3-kinase activity in frog skeletal muscle. *Comp. Biochem. Physiol. B Biochem. Mol. Biol.* 110:747–753.

Cognard, C., M. Rivet, and G. Raymond. 1990. The blockade of excitation/contraction coupling by nifedipine in patch-clamped rat skeletal muscle cells in culture. *Pflugers Arch.* 416:98–105.

De Smedt, H., L. Missiaen, J.B. Parys, R.H. Henning, I. Sienaert, S. Vanlingen, A. Gijsens, B. Himpens, and R. Casteels. 1997. Isoform diversity of the inositol trisphosphate receptor in cell types of mouse origin. *Biochem. J.* 322(Pt 2):575–583.

Deconinck, N., T. Ragot, G. Marechal, M. Perricaudet, and J.M. Gillis. 1996. Functional protection of dystrophic mouse (mdx) muscles after adenovirus-mediated transfer of a dystrophin minigene. *Proc. Natl. Acad. Sci. USA.* 93:3570–3574.

Divet, A., and C. Huchet-Cadiou. 2002. Sarcoplasmic reticulum function in slow- and fast-twitch skeletal muscles from mdx mice. *Pflugers Arch.* 444:634–643.

Dyer, J.L., and F. Michelangeli. 2001. Inositol 1,4,5-trisphosphate receptor isoforms show similar Ca^{2+} release kinetics. *Cell Calcium.* 30:245–250.

Ervasti, J.M., and K.P. Campbell. 1991. Membrane organization of the dystrophin-glycoprotein complex. *Cell.* 66:1121–1131.

Estrada, M., C. Cardenas, J.L. Liberona, M.A. Carrasco, G.A. Mignery, P.D. Allen, and E. Jaimovich. 2001. Calcium transients in 1B5 myotubes lacking ryanodine receptors are related to inositol trisphosphate receptors. *J. Biol. Chem.* 276:22868–22874.

Franzini-Armstrong, C., and J.W. Kish. 1995. Alternate disposition of tetrads in peripheral couplings of skeletal muscle. *J. Muscle Res. Cell Motil.* 16:319–324.

Furuichi, T., and K. Mikoshiba. 1995. Inositol 1, 4, 5-trisphosphate receptor-mediated Ca^{2+} signalling in the brain. *J. Neurochem.* 64:953–960.

Hidalgo, C., M.A. Carrasco, K. Magendzo, and E. Jaimovich. 1986. Phosphorylation of phosphatidylinositol by transverse tubule vesicles and its possible role in excitation-contraction coupling. *FEBS Lett.* 202:69–73.

Hoffman, E.P., R.H. Brown Jr., and L.M. Kunkel. 1987. Dystrophin: the protein product of the Duchenne muscular dystrophy locus. *Cell.* 51:919–928.

Imbert, N., C. Cognard, G. Duport, C. Guillou, and G. Raymond. 1995. Abnormal calcium homeostasis in Duchenne muscular dystrophy myotubes contracting in vitro. *Cell Calcium.* 18:177–186.

Imbert, N., C. Vandebrouck, B. Constantin, G. Duport, C. Guillou, C. Cognard, and G. Raymond. 1996. Hypoosmotic shocks induce elevation of resting calcium level in Duchenne muscular dystrophy myotubes contracting in vitro. *Neuromuscul. Disord.* 6:351–360.

Imbert, N., C. Vandebrouck, G. Duport, G. Raymond, A.A. Hassoni, B. Constantin, M.J. Cullen, and C. Cognard. 2001. Calcium currents and transients in co-cultured contracting normal and Duchenne muscular dystrophy human myotubes. *J. Physiol.* 534:343–355.

Jaimovich, E., R. Reyes, J.L. Liberona, and J.A. Powell. 2000. IP(3) receptors, IP(3) transients, and nucleus-associated Ca^{2+} signals in cultured skeletal muscle. *Am. J. Physiol. Cell Physiol.* 278: C998–C1010.

Kanthou, C., S.M. Kanse, V.V. Kakkar, and O. Benzakour. 1996. Involvement of pertussis toxin-sensitive and -insensitive G proteins in α-thrombin on cultured human vascular smooth muscle cells. *Cell. Signal.* 8:59–66.

Lampe, P.D., Q. Qiu, R.A. Meyer, E.M. TenBroek, T.F. Walseth, T.A. Starich, H.L. Grunenwald, and R.G. Johnson. 2001. Gap junction assembly: PTX-sensitive G proteins regulate the distribution of connexin43 within cells. *Am. J. Physiol. Cell Physiol.* 281: C1211–C1222.

Liberona, J.L., J.A. Powell, S. Shenoi, L. Petherbridge, R. Caviedes, and E. Jaimovich. 1998. Differences in both inositol 1,4,5-trisphosphate mass and inositol 1,4,5-trisphosphate receptors between normal and dystrophic skeletal muscle cell lines. *Muscle Nerve.* 21:902–909.

Lipp, P., M. Laine, S.C. Tovey, K.M. Burrell, M.J. Berridge, W. Li, and M.D. Bootman. 2000. Functional InsP3 receptors that may modulate excitation-contraction coupling in the heart. *Curr. Biol.* 10:939–942.

Lorenzon, N.M., C.S. Haarmann, E.E. Norris, S. Papadopoulos, and K.G. Beam. 2004. Metabolic biotinylation as a probe of supramolecular structure of the triad junction in skeletal muscle. *J. Biol. Chem.* 279:44057–44064.

Mackenzie, L., M.D. Bootman, M. Laine, M.J. Berridge, J. Thuring, A. Holmes, W.H. Li, and P. Lipp. 2002. The role of inositol 1,4,5-trisphosphate receptors in Ca^{2+} signalling and the generation of arrhythmias in rat atrial myocytes. *J. Physiol.* 541:395–409.

Marchand, E., B. Constantin, H. Balghi, M.C. Claudepierre, A. Cantereau, C. Magaud, A. Mouzou, G. Raymond, S. Braun, and C. Cognard. 2004. Improvement of calcium handling and changes in calcium-release properties after mini- or full-length dystrophin forced expression in cultured skeletal myotubes. *Exp. Cell Res.* 297:363–379.

Miyakawa, T., A. Maeda, T. Yamazawa, K. Hirose, T. Kurosaki, and M. Iino. 1999. Encoding of Ca^{2+} signals by differential expression of IP3 receptor subtypes. *EMBO J.* 18:1303–1308.

Monaco, A.P., R.L. Neve, C. Colletti-Feener, C.J. Bertelson, D.M. Kurnit, and L.M. Kunkel. 1986. Isolation of candidate cDNAs for portions of the Duchenne muscular dystrophy gene. *Nature.* 323:646–650.

Mulle, C., P. Benoit, C. Pinset, M. Roa, and J.P. Changeux. 1988. Calcitonin gene-related peptide enhances the rate of desensitization of the nicotinic acetylcholine receptor in cultured mouse muscle cells. *Proc. Natl. Acad. Sci. USA.* 85:5728–5732.

Patel, S., S.K. Joseph, and A.P. Thomas. 1999. Molecular properties of inositol 1,4,5-trisphosphate receptors. *Cell Calcium.* 25:247–264.

Powell, J.A., M.A. Carrasco, D.S. Adams, B. Drouet, J. Rios, M. Muller, M. Estrada, and E. Jaimovich. 2001. IP(3) receptor

function and localization in myotubes: an unexplored Ca^{2+} signalling pathway in skeletal muscle. *J. Cell Sci.* 114:3673–3683.

Protasi, F., C. Paolini, J. Nakai, K.G. Beam, C. Franzini-Armstrong, and P.D. Allen. 2002. Multiple regions of RyR1 mediate functional and structural interactions with α1S-dihydropyridine receptors in skeletal muscle. *Biophys. J.* 83:3230–3244.

Reyes, R., and E. Jaimovich. 1996. Functional muscarinic receptors in cultured skeletal muscle. *Arch. Biochem. Biophys.* 331:41–47.

Rios, E., J.J. Ma, and A. Gonzalez. 1991. The mechanical hypothesis of excitation-contraction (EC) coupling in skeletal muscle. *J. Muscle Res. Cell Motil.* 12:127–135.

Salanova, M., G. Priori, V. Barone, E. Intravaia, B. Flucher, F. Ciruela, R.A. McIlhinney, J.B. Parys, K. Mikoshiba, and V. Sorrentino. 2002. Homer proteins and InsP(3) receptors co-localise in the longitudinal sarcoplasmic reticulum of skeletal muscle fibres. *Cell Calcium.* 32:193–200.

Ursu, D., S. Sebille, B. Dietze, D. Freise, V. Flockerzi, and W. Melzer. 2001. Excitation-contraction coupling in skeletal muscle of a mouse lacking the dihydropyridine receptor subunit γ1. *J. Physiol.* 533:367–377.

Vandebrouck, C., G. Duport, C. Cognard, and G. Raymond. 2001. Cationic channels in normal and dystrophic human myotubes. *Neuromuscul. Disord.* 11:72–79.

Vandebrouck, C., D. Martin, M. Colson-Van Schoor, H. Debaix, and P. Gailly. 2002. Involvement of TRPC in the abnormal calcium influx observed in dystrophic (mdx) mouse skeletal muscle fibers. *J. Cell Biol.* 158:1089–1096.

Zhou, Y.W., S.A. Oak, S.E. Senogles, and H.W. Jarret. 2005. Laminin-α_1 globular domains 3 and 4 induce heterotrimeric G protein binding to α-syntrophin's PDZ domain and alter intracellular Ca^{2+} in muscle. *Am. J. Physiol. Cell Physiol.* 288:C377–C388.